Scientia Iranica A (2012) 19 (4), 1033–1043

Sharif University of Technology

Scientia Iranica

Transactions A: Civil Engineering

www.sciencedirect.com

Research note

Determination of ultimate load and possible failure path for solid continuous media using adaptive refinement process

A. Asghari [a,*], **R. Mirghaderi** [b]

[a] *Department of Civil Engineering, Urmia University of Technology, Urmia, P.O. Box: 57155-419, Iran*
[b] *School of Civil Engineering, College of Engineering, University of Tehran, Tehran, P.O. Box: 11365-4563, Iran*

Received 11 August 2011; revised 12 February 2012; accepted 17 June 2012

KEYWORDS

Adaptive refinement;
Rule of gradient recovery;
Error norm;
Adaptive finite element method;
Error post-processor;
Discretization;
J norm.

Abstract In this study, an effective and practical, *h*-version, enrichment mesh generation, and finite element adaptive procedure for the non-linear solution of problems in continuous media is presented. Moreover, based on the gradient recovery rule, a general recovery technique is developed to measure error and refine mesh in general finite element solutions. The recovery technique is simple and cost effective to implement. The technique has been formulated for two dimensional problems by employing triangular elements. The formulation is consistent with non-linear formulations which iteratively equilibrate the continuous media problems.

In the present study, in addition to correlating various norms (such as energy norm, L_2 norm for stress and L_2 norm for strain), a new norm, namely, deviating stresses norm (called ***J*** norm in this study), is also correlated by the authors to estimate the error rate in the finite element method. Based on the results of this study, the ***J*** norm can be used as a tool to estimate the error rate in the finite element method, and to determine the ultimate load and the possible failure path in continuous domains. For several numerical examples, the developed algorithms are demonstrated and the resulting meshes are presented.

1. Introduction

Since the beginning of modeling physical events by computers, numerical errors have been the main cause of concern. Numerical and computational errors are the main characteristics of these types of modeling. In the discretization process of the mechanical behavior of continuous domains into a controllable model by differential equations or by integration on computers, it is impossible to place all information in the model. In addition, most results obtained from classical methods are an unlimited series, which lead to approximate responses. In such cases, the finite element method is firmly accepted as one of the most powerful general techniques for the numerical solution of a variety of problems encountered in engineering.

In the finite element method, the continuous domain is divided into simple and smaller geometrical elements, called finite elements, and the unknown parameters are computed, with respect to their order of position, by satisfying compatibility, fundamental equations and equilibrium equations. However, there are almost no accessible tools for engineers to select suitable element sizes and proper solutions. Moreover, each element size is selected based on expert judgments in such a way that the number of degrees of freedom in continuous media is occasionally so large that solution by ordinary software becomes uneconomical or impossible. In the last two decades, significant advances have been made to overcome the weaknesses in the finite element method. One can use adaptive finite element methods based on recovery methods.

Error estimation in the finite element method primarily received attention in Rheinboldt and Babuska's innovative work in 1978–1983 to solve elliptic boundary value problems [1,2]. In the early 1980s, Demkowicz, Bank and Weiser's research on recovery methods resulted in an extensive range of error

* Corresponding author.
E-mail addresses: a.asghari.69@gmail.com (A. Asghari), rmirghaderi@ut.ac.ir (R. Mirghaderi).

Peer review under responsibility of Sharif University of Technology.

Production and hosting by Elsevier

1026-3098 © 2012 Sharif University of Technology. Production and hosting by Elsevier B.V. Open access under CC BY-NC-ND license.
doi:10.1016/j.scient.2012.06.005

estimators [3]. In the late 1980s, Zhu and Zienkiewicz presented a simple error estimator and adaptive procedure for practical engineering analysis [4]. In the early 1990s, the post-processing of error was established and then was directed to general problems. Most methods presented during these years are considered "recovery-based methods". In recovery methods, using the concept of error norm, the error value is evaluated by comparison of the finite element approximation gradients and smoothed the real gradients in each element [5–9].

The other approach was introduced in 1987 by Zienkiewicz and Zhu, which estimated the error in gradient (or stress) based norms, simply by obtaining the improved values of the gradient using several available recovery processes. In the earliest works, a so called L_2 projection and an even simpler averaging procedure were used, yielding quite acceptable estimates. However, in 1992, an important step forward was made by introduction of the Superconvergent Patch Recovery (SPR) technique by the same authors. As the name of the technique implies, it makes use of special points in the finite element model (such as the Gauss quadrature points), where derivatives of the finite element solutions exhibit higher accuracy compared to that normally expected [10–12]. In 1997, Boroomand and Zienkiewicz improved the SPR recovery method to the REP (Recovery by Equilibrium in Patches) method. This method avoids the specification of superconvergent points, which in fact do not exist in a number of families of the finite element (e.g. triangles). The formulation of REP is simple and is based on using a weighted form of the equilibrium condition over representative patches of elements [13,14].

Currently, the post-processing of errors has reached its maturity and much attention has been focused on developing new methods and determining their performance scopes. A large number of studies have been carried out related to the post-processing of errors to determine the errors in finite element approximations [15].

In the present study, the authors have used the Von Mises yield criterion ($\boldsymbol{J}$ norm) in the error estimation process, and the *h*-refinement strategy in the adaptive finite element method, in order to present an efficient simple tool to overcome weaknesses in the general finite element method. It is given that in these non-linear solutions, element size selection is intelligent and rational; furthermore, discretization of the whole domain is prevented. Hence, the solution operations suggested in this paper have been reduced to a great extent, which is recommended for engineering applications. Besides, based on the method used in this study, it becomes possible to access failure bond propagation as well as the formation and failure mechanism type. In addition, using directional error, a modified *h*-method (subdivision size, which is a natural way for most engineers) is presented, which can be applied to obtain acceptable solution accuracy and simultaneously reduce computational time.

2. Fundamental equations

An extensive range of boundary value problems, including all problems of linear elasticity, are characterized by the following equation:

$$\boldsymbol{Lu} - \boldsymbol{b} = 0 \equiv \boldsymbol{S}^{\boldsymbol{T}}\boldsymbol{DSu} - \boldsymbol{b} = 0 \quad \text{in domain } \Omega, \tag{1}$$

and appropriate boundary conditions:

$$\boldsymbol{u} = \bar{\boldsymbol{u}}_{\Gamma} \quad \text{on } \Gamma_u, \tag{2}$$

$$\boldsymbol{t} = \boldsymbol{G\sigma} = \boldsymbol{GDSu} = \bar{\boldsymbol{t}}_{\Gamma} \quad \text{on } \Gamma_t, \tag{3}$$

$$\text{with } \Gamma_u U \Gamma_t = \Gamma, \tag{4}$$

where:

$\boldsymbol{L}$ = linear differential operator,
$\boldsymbol{S}$ = strain differential operator,
$\boldsymbol{D}$ = elasticity matrix,
$\boldsymbol{b}$ = body forces,
$\boldsymbol{u}$ = exact displacement vector (in elasticity, of course, $\boldsymbol{u}$ corresponds to a generalized displacement),
$\boldsymbol{\sigma}$ = exact stress vector,
$\boldsymbol{G}$ = linear differential operator,
$\boldsymbol{t}$ = traction vectors,
Ω = domain,
Γ = boundary of domain,
Γ_u = part of the boundary where displacement conditions are specified,
Γ_t = part of the boundary where traction conditions are specified,
$\bar{\boldsymbol{u}}_{\Gamma}$ = prescribed displacements on the Γ_u boundary,
$\bar{\boldsymbol{t}}_{\Gamma}$ = prescribed tractions on the Γ_t boundary.

We shall denote by $\boldsymbol{u}_h$ the finite element approximation to the exact solution, $\boldsymbol{u}$, obtained by standard Galerkin procedure, and written as:

$$\boldsymbol{u} \approx \boldsymbol{u}_h = \boldsymbol{N}\bar{\boldsymbol{u}}, \tag{5}$$

the directly computed consistent, stresses, (or gradients) are:

$$\boldsymbol{\sigma}_h = \boldsymbol{D\varepsilon}_h = \boldsymbol{DSu}_h = \boldsymbol{DSN}\bar{\boldsymbol{u}} = \boldsymbol{DB}\bar{\boldsymbol{u}}, \tag{6}$$

where, $\bar{\boldsymbol{u}}$ is assigned as the nodal value of the displacements, $\boldsymbol{N}$ is denoted as the finite element basis functions, and $\boldsymbol{S}$ is designated as the differential operator which defines the strain as:

$$\boldsymbol{\varepsilon}_h = \boldsymbol{Su}_h = \boldsymbol{SN}\bar{\boldsymbol{u}} = \boldsymbol{B}\bar{\boldsymbol{u}}, \tag{7}$$

$\boldsymbol{B}$ is assigned as the strain–displacement matrix, and $\boldsymbol{N}$ is denoted as the shape functions.

By using the principle of virtual work in a standard *FE* manner, the alternative form of equilibrium equations can be written as:

$$\boldsymbol{K}\bar{\boldsymbol{u}} - \boldsymbol{f} = 0, \tag{8}$$

where:

$$\boldsymbol{K} = \int_{\Omega} (\boldsymbol{SN})^T \boldsymbol{D}(\boldsymbol{SN})\, d\Omega = \int_{\Omega} \boldsymbol{B}^T \boldsymbol{DB}\, d\Omega \quad \text{and} \quad \boldsymbol{B} = \boldsymbol{SN}. \tag{9}$$

In Eq. (8), parameter $\boldsymbol{f}$ represents a 'force' vector incorporating the body forces, $\boldsymbol{b}$, and the boundary conditions. Parameter $\boldsymbol{f}$ can be computed as:

$$\boldsymbol{f} = \int_{\Omega} \boldsymbol{N}^T \boldsymbol{b}\, d\Omega + \int_{\Gamma_t} \boldsymbol{N}^T \boldsymbol{t}\, d\Gamma. \tag{10}$$

After assembling the stiffness matrix of all elements and forming the nodal forces vector, $\bar{\boldsymbol{u}}$ and $\boldsymbol{u}_h$ values are calculated by solving a number of simultaneous equations. The stress of the finite element approximation is further obtained by the following equations:

$$\boldsymbol{\sigma}_h = \boldsymbol{DB}\bar{\boldsymbol{u}}. \tag{11}$$

The finite element method solutions have several limitations as follows:

1. Lack of awareness of suitable element size.
2. Lack of awareness of correct solution and error rate.
3. Lack of precise information about displacement provided.
4. Lack of awareness of the value of error made in the process of discretization.
5. Lack of information about propagation of a possible failure path.
6. Costly access to the occurrence path of the failure mechanism; this is because the size of elements used are usually equal, and access to the occurrence path of the failure mechanism is highly complex.

3. Error estimation

Since the finite element method is merely an approximate method to solve continuous domains accurately, there is constantly a difference between the finite element approximation and the exact response. Therefore, if $\boldsymbol{u}_h$ and $\boldsymbol{\sigma}_h$ represent the finite element approximation and $\boldsymbol{u}$ and $\boldsymbol{\sigma}$ represent the exact responses, the error of the finite element approximation, $\boldsymbol{u}_h$, with respect to the exact solution, $\boldsymbol{u}$, can be defined as [4]:

$$\boldsymbol{e} = \boldsymbol{u} - \boldsymbol{u}_h. \tag{12}$$

And the error of the stresses (gradient) is defined as:

$$\boldsymbol{e}_\sigma = \boldsymbol{\sigma} - \boldsymbol{\sigma}_h. \tag{13}$$

A point wise definition of error, as given in Eqs. (12) and (13), is generally difficult to specify, and various integral measures are more conveniently adopted. One of the most common of such measures is the 'energy norm', written for a general problem and which, in the specific case of elasticity, is presented as [5–7]:

$$\|\boldsymbol{u}\| = \left[\int_\Omega \boldsymbol{u}^T \boldsymbol{L}\boldsymbol{u}\, d\Omega\right]^{1/2} = \left[\int_\Omega \boldsymbol{\sigma}^T \boldsymbol{D}^{-1}\boldsymbol{\sigma}\, d\Omega\right]^{1/2}, \tag{14}$$

where, Ω is the domain on which the problem is defined and $\boldsymbol{D}$ is the elasticity matrix. The energy norm of $\boldsymbol{e}$ is written as:

$$\begin{aligned}\|\boldsymbol{e}\| &= \left[\int_\Omega \boldsymbol{e}^T \boldsymbol{L}\boldsymbol{e}\, d\Omega\right]^{1/2},\\ &= \left[\int_\Omega (\boldsymbol{S}\boldsymbol{e})^T \boldsymbol{D}(\boldsymbol{S}\boldsymbol{e})\, d\Omega\right]^{1/2},\\ &= \left[\int_\Omega (\boldsymbol{e}_\varepsilon)^T \boldsymbol{D}(\boldsymbol{e}_\varepsilon)\, d\Omega\right]^{1/2},\\ &= \left[\int_\Omega (\boldsymbol{\sigma} - \boldsymbol{\sigma}_h)^T \boldsymbol{D}^{-1}(\boldsymbol{\sigma} - \boldsymbol{\sigma}_h)\, d\Omega\right]^{1/2}.\end{aligned} \tag{15}$$

In the above equations, $\boldsymbol{S}$ is the strain operator and $\boldsymbol{\sigma}^T$ and $\boldsymbol{\sigma}_h^T$ vectors are defined as:

$$\boldsymbol{\sigma}^T = \begin{Bmatrix}\sigma_x & \sigma_y & \sigma_{xy}\end{Bmatrix} \quad \text{and} \quad \boldsymbol{\sigma}_h^T = \begin{Bmatrix}\sigma_{xh} & \sigma_{yh} & \sigma_{xyh}\end{Bmatrix}. \tag{16}$$

Although the absolute value of the energy norm has little physical meaning, the relative percentage error, e.g;

$$\eta = \left[\frac{\|\boldsymbol{e}\|^2}{\|\boldsymbol{u}\|^2 + \|\boldsymbol{e}\|^2}\right]^{1/2} \times 100\%, \tag{17}$$

is more easily interpreted. The percentage error, η, can be determinate for the whole domain or for the element subdomains. The local definition is obviously more meaningful.

A more direct measure is the so called L_2 norm, which can be associated with the errors in any quantity. Thus, for the displacement, $\boldsymbol{u}$, the L_2 norm of the error, $\boldsymbol{e}$, can be written as:

$$\|\boldsymbol{e}\|_{L_2} = \left[\int_\Omega \boldsymbol{e}^T \boldsymbol{e} d\Omega\right]^{1/2}, \tag{18}$$

and for stresses:

$$\|\boldsymbol{e}_\sigma\|_{L_2} = \left[\int_\Omega (\boldsymbol{e}_\sigma)^T (\boldsymbol{e}_\sigma)\, d\Omega\right]^{1/2}. \tag{19}$$

The latter expression differing from the energy norm only by the weighting, $\boldsymbol{D}^{-1}$.

Based on the research performed in this area, although using different norms to estimate the error caused by the finite element solution generate nearly identical results, the authors of this paper have attempted to involve yield criteria concepts, such as von Mises, Tresca, Mohr–Coulomb, and others, in estimating the error. In this study, in addition to the energy norm, the $\boldsymbol{J}$ norm, which is derived from the Von Mises criterion, was used as well [16]. The vector, $\boldsymbol{S}_\sigma$, is defined in order to correlate the $\boldsymbol{J}$ norm as below:

$$\boldsymbol{S}_\sigma^T = \begin{Bmatrix}S_x & S_y & S_{xy}\end{Bmatrix}. \tag{20}$$

S_x, S_y, and S_{xy} are being set in such a way that the result of $\boldsymbol{S}_\sigma^T\boldsymbol{S}_\sigma$, which is $(\boldsymbol{S}_x^2 + \boldsymbol{S}_y^2 + \boldsymbol{S}_{xy}^2)$, leads to $\boldsymbol{J}_2$, where $\boldsymbol{J}_2$ is the second invariant of the stress deviator tensor. For plane stress conditions, $\boldsymbol{J}_2$ can be computed by the following equations:

$$\begin{aligned}\boldsymbol{J}_2 &= \frac{1}{6}[(\sigma_x - \sigma_y)^2 + (\sigma_y - \sigma_z)^2\\ &\quad + (\sigma_z - \sigma_x)^2] + \sigma_{xy}^2 + \sigma_{yz}^2 + \sigma_{zx}^2\\ &= \frac{1}{6}[(\sigma_x - \sigma_y)^2 + \sigma_y^2 + \sigma_x^2] + \sigma_{xy}^2\\ &= \frac{1}{6}[\sigma_x^2 + \sigma_y^2 - 2\sigma_x\sigma_y + \sigma_x^2 + \sigma_y^2] + \sigma_{xy}^2\\ &= \frac{1}{3}(\sigma_x - \sigma_y)^2 + \frac{1}{3}\sigma_x\sigma_y + \sigma_{xy}^2.\end{aligned} \tag{21}$$

According to the last of Expression (21), $\boldsymbol{S}_\sigma^T$ vector can be adjusted as:

$$\boldsymbol{S}_\sigma^T = \left\{\frac{(\boldsymbol{\sigma}_x - \boldsymbol{\sigma}_y)}{\sqrt{3}} \quad \sqrt{\left(\frac{1}{3}\boldsymbol{\sigma}_x \cdot \boldsymbol{\sigma}_y\right)} \quad \boldsymbol{\sigma}_{xy}\right\}. \tag{22}$$

For linear elasticity problems, the $\boldsymbol{J}$ norm and the $\boldsymbol{J}$ norm of $\boldsymbol{e}$ can be defined as:

$$\|\boldsymbol{J}\| = \left[\int_\Omega \boldsymbol{S}_\sigma^T \boldsymbol{S}_\sigma\, d\Omega\right]^{1/2}, \tag{23}$$

$$\|\boldsymbol{e}\| = \left[\int_\Omega (\boldsymbol{S}_\sigma - \boldsymbol{S}_{\sigma h})^T (\boldsymbol{S}_\sigma - \boldsymbol{S}_{\sigma h})\, d\Omega\right]^{1/2}. \tag{24}$$

Similarly, the relative percentage error in the $\boldsymbol{J}$ norm is written as:

$$\eta = \left[\frac{\|\boldsymbol{e}\|^2}{\|\boldsymbol{J}\|^2 + \|\boldsymbol{e}\|^2}\right]^{1/2} \times 100\%. \tag{25}$$

Error estimation by Eqs. (17) and (25) is possible only if the exact solutions are available. However, since the exact solutions, $\boldsymbol{u}$ and $\boldsymbol{\sigma}$, are obviously not available in practical computations to evaluate errors, we seek several practical and effective methods to estimate $\boldsymbol{e}$ in an appropriate norm. An efficient and simple method to access exact solutions and estimate the error value is the derivative recovery technique.

Approximate solutions of second-order partial differential equations by the Galerkin finite element method typically result in discontinuous derivatives. For example, in elastic solutions, the displacements are continuous; however, the derivatives of displacement, stress and strain, are not. The derivative recovery techniques are motivated by the need to post-process the results from finite element solutions.

According to the derivative recovery technique, the stress, $\boldsymbol{\sigma}$,can be represented more accurately by a smooth field, $\boldsymbol{\sigma}^*$,

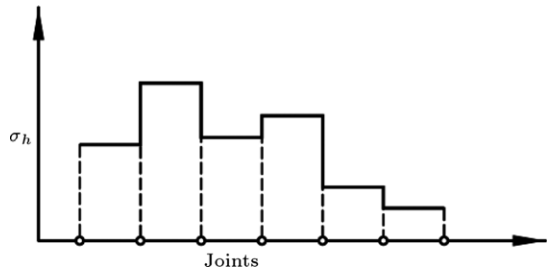

Figure 1: Stress of finite element solution for part of a continuous media.

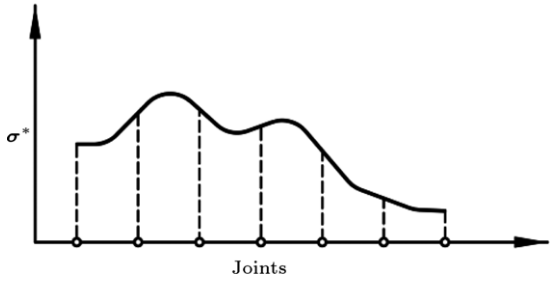

Figure 2: Smoothed stress by the rule of gradient recovery for part of a continuous media.

interpolated by continuous shape function, $\boldsymbol{N}_\sigma$, and unknown nodal parameters, $\bar{\boldsymbol{\sigma}}$, as:

$$\boldsymbol{\sigma}^* = \boldsymbol{N}_\sigma \cdot \bar{\boldsymbol{\sigma}}. \tag{26}$$

The interpolation functions, $\boldsymbol{N}_\sigma$, are used as the best selection to be of the same order as the shape function, $\boldsymbol{N}$. Further, frequently, we have:

$$\boldsymbol{N}_\sigma = \boldsymbol{N} \Rightarrow \boldsymbol{\sigma}^* = \boldsymbol{N} \cdot \bar{\boldsymbol{\sigma}}. \tag{27}$$

Figures 1 and 2 present the stress of the finite element solution and smoothed stress by the rule of gradient recovery for part of a continuous media, respectively.

It is intuitively 'obvious' that $\boldsymbol{\sigma}^*$ is, in fact, a better approximation than $\boldsymbol{\sigma}_h$ and is used to estimate error $\boldsymbol{e}_\sigma$ (namely, Eq. (1)), i.e. put

$$\boldsymbol{e}_\sigma \approx \boldsymbol{\sigma}^* - \boldsymbol{\sigma}_h, \tag{28}$$

to find nodal parameters, $\bar{\boldsymbol{\sigma}}$. The error norm for the stress of finite element approximation and smoothed stresses by the rule of gradient recovery can be used in the entire domain [16].

$$F(\bar{\boldsymbol{\sigma}}) = \langle \boldsymbol{\sigma}^*, \boldsymbol{\sigma}_h \rangle = \int_\Omega (\boldsymbol{\sigma}^* - \boldsymbol{\sigma}_h)^2 \, d\Omega, \tag{29}$$

$$F(\bar{\boldsymbol{\sigma}}) = \int_\Omega (\boldsymbol{N}\bar{\boldsymbol{\sigma}} - \boldsymbol{\sigma}_h)^2 \, d\Omega, \tag{30}$$

$$\partial F(\bar{\boldsymbol{\sigma}})/\partial \bar{\boldsymbol{\sigma}} = 0 \Rightarrow \int_\Omega \boldsymbol{N}^T \cdot (\boldsymbol{N}\bar{\boldsymbol{\sigma}} - \boldsymbol{\sigma}_h) \, d\Omega = 0, \tag{31}$$

$$\int_\Omega \boldsymbol{N}^T \cdot \boldsymbol{N}\bar{\boldsymbol{\sigma}} \, d\Omega = \int_\Omega \boldsymbol{N}^T \cdot \boldsymbol{\sigma}_h \, d\Omega, \tag{32}$$

$$\left[\int_\Omega \boldsymbol{N}^T \cdot \boldsymbol{N} \, d\Omega\right] \cdot \bar{\boldsymbol{\sigma}} = \int_\Omega \boldsymbol{N}^T \cdot \boldsymbol{\sigma}_h \, d\Omega. \tag{33}$$

If Eq. (33) is represented as follows, then:

$$\boldsymbol{M} \cdot \bar{\boldsymbol{\sigma}} = P, \tag{34}$$

$$\boldsymbol{M} = \int_\Omega \boldsymbol{N}^T \cdot \boldsymbol{N} \, d\Omega, \tag{35}$$

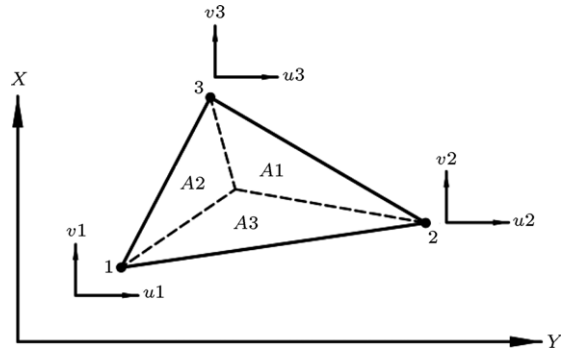

Figure 3: Area coordinates system and nodal points of three-node triangular element.

$$\boldsymbol{P} = \int_\Omega \boldsymbol{N}^T \cdot \boldsymbol{\sigma}_h \, d\Omega. \tag{36}$$

Since the elements used in the present work are three-node triangular elements (see Figure 3), and if the area coordinate systems without any dimension are selected, displacement shape functions are computed as follows:

$$L_1 = \frac{A1}{A}, \qquad L_2 = \frac{A2}{A}, \qquad L_3 = \frac{A3}{A}, \tag{37}$$

$$L_1 + L_2 + L_3 = 1, \tag{38}$$

$$\boldsymbol{N} = \begin{Bmatrix} L_1 & L_2 & L_3 \end{Bmatrix}, \tag{39}$$

$$\boldsymbol{\sigma}_h = \begin{Bmatrix} \boldsymbol{\sigma}_{xh} \\ \boldsymbol{\sigma}_{yh} \\ \boldsymbol{\sigma}_{xyh} \end{Bmatrix} = \text{constant}. \tag{40}$$

Since the nodal stresses, $\bar{\boldsymbol{\sigma}}_x$, $\bar{\boldsymbol{\sigma}}_y$ and $\bar{\boldsymbol{\sigma}}_{xy}$, are independent, calculations for $\bar{\boldsymbol{\sigma}}_x$, $\bar{\boldsymbol{\sigma}}_y$ and $\bar{\boldsymbol{\sigma}}_{xy}$ are carried out separately. Therefore, using the presented shape functions, matrix $[\boldsymbol{M}]$ and vector $\{\boldsymbol{P}\}$ can be computed by the following equations:

$$[\boldsymbol{M}]_i = \begin{bmatrix} 2 & 1 & 1 \\ 1 & 2 & 1 \\ 1 & 1 & 2 \end{bmatrix} \times \frac{Ai}{12}, \tag{41}$$

$$\{\boldsymbol{P}_x\}_i = \begin{Bmatrix} 1 \\ 1 \\ 1 \end{Bmatrix} \times \boldsymbol{\sigma}_{xh} \times \frac{Ai}{3}, \tag{42}$$

$$\{\boldsymbol{P}_y\}_i = \begin{Bmatrix} 1 \\ 1 \\ 1 \end{Bmatrix} \times \boldsymbol{\sigma}_{yh} \times \frac{Ai}{3}, \tag{43}$$

$$\{\boldsymbol{P}_{xy}\}_i = \begin{Bmatrix} 1 \\ 1 \\ 1 \end{Bmatrix} \times \boldsymbol{\sigma}_{xyh} \times \frac{Ai}{3}. \tag{44}$$

After forming matrix $[\boldsymbol{M}]_i$ and vectors $\{\boldsymbol{P}_x\}_i$, $\{\boldsymbol{P}_y\}_i$ and $\{\boldsymbol{P}_{xy}\}_i$ for all elements and adding them together, $\bar{\boldsymbol{\sigma}}_x$, $\bar{\boldsymbol{\sigma}}_y$ and $\bar{\boldsymbol{\sigma}}_{xy}$ are calculated for all nodes by solving several simultaneous equations.

$$[\boldsymbol{M}] \cdot \{\bar{\boldsymbol{\sigma}}_x\} = \{\boldsymbol{P}_x\} \Rightarrow \{\bar{\boldsymbol{\sigma}}_x\} = [\boldsymbol{M}]^{-1} \cdot \{\boldsymbol{P}_x\}, \tag{45}$$

$$[\boldsymbol{M}] \cdot \{\bar{\boldsymbol{\sigma}}_y\} = \{\boldsymbol{P}_y\} \Rightarrow \{\bar{\boldsymbol{\sigma}}_y\} = [\boldsymbol{M}]^{-1} \cdot \{\boldsymbol{P}_y\}, \tag{46}$$

$$[\boldsymbol{M}] \cdot \{\bar{\boldsymbol{\sigma}}_{xy}\} = \{\boldsymbol{P}_{xy}\} \Rightarrow \{\bar{\boldsymbol{\sigma}}_{xy}\} = [\boldsymbol{M}]^{-1} \cdot \{\boldsymbol{P}_{xy}\}. \tag{47}$$

It has been noted that, in practice, the smoothed approximation of the stress is generally more accurate than $\boldsymbol{\sigma}_h$. The error estimator is obtained simply by arguing that substituting smoothed stress $\boldsymbol{\sigma}^*$ for true stress $\boldsymbol{\sigma}$ in Eqs. (14) and (15) should yield a reasonable approximation to the error in the energy norm. In

fact, this has been observed to be the case in practice, and examples illustrating the effectiveness of this process are presented in Section 6. Therefore, the error value in the energy norm is computed based on the rule of gradient recovery as follows:

$$\left\|\boldsymbol{u}^*\right\| = \left[\int_{\Omega} \boldsymbol{\sigma}^{*T}\boldsymbol{D}^{-1}\boldsymbol{\sigma}^* \, d\Omega\right]^{1/2}, \tag{48}$$

$$\left\|\boldsymbol{e}^*\right\| = \left[\int_{\Omega} (\boldsymbol{\sigma}^* - \boldsymbol{\sigma}_h)^T\boldsymbol{D}^{-1}(\boldsymbol{\sigma}^* - \boldsymbol{\sigma}_h) \, d\Omega\right]^{1/2}, \tag{49}$$

and the relative percentage error can be written as:

$$\eta = \left[\frac{\|\boldsymbol{e}^*\|^2}{\|\boldsymbol{u}^*\|^2 + \|\boldsymbol{e}^*\|^2}\right]^{1/2} \times 100\%. \tag{50}$$

Therefore, the error value in the $\boldsymbol{J}$ norm can be computed as follows:

$$\left\|\boldsymbol{J}^*\right\| = \left[\int_{\Omega} \boldsymbol{S}_{\sigma}^{*T}\boldsymbol{S}_{\sigma}^* \, d\Omega\right]^{1/2}, \tag{51}$$

$$\left\|\boldsymbol{e}_{\boldsymbol{J}}^*\right\| = \left[\int_{\Omega} (\boldsymbol{S}_{\sigma}^* - \boldsymbol{S}_{\sigma h})^T(\boldsymbol{S}_{\sigma}^* - \boldsymbol{S}_{\sigma h}) \, d\Omega\right]^{1/2}, \tag{52}$$

and the relative percentage error in the $\boldsymbol{J}$ norm can be expressed as:

$$\eta = \left[\frac{\left\|\boldsymbol{e}_{\boldsymbol{J}}^*\right\|^2}{\left\|\boldsymbol{J}^*\right\|^2 + \left\|\boldsymbol{e}_{\boldsymbol{J}}^*\right\|^2}\right]^{1/2} \times 100\%, \tag{53}$$

where $\boldsymbol{S}_{\sigma}^*$ and $\boldsymbol{S}_{\sigma h}$ are calculated as Eq. (22).

Hence, it is required that after the final analysis is completed, the condition:

$$\eta < \bar{\eta}, \tag{54}$$

should be satisfied for the whole domain, where $\bar{\eta}$ is the maximum permissible error. In practical conditions, $\bar{\eta}$ is considered to be less than 10%. If $\eta > \bar{\eta}$, the error is more than the permissible error and mesh generation ought to be refined to obtain an acceptable response.

4. Error estimation for each element and refinement strategy

In the previous section, the overall relative percentage error (η) of the entire domain was computed. To reach the permissible error, the first solution which comes to mind is to make all elements smaller, until $\eta < \bar{\eta}$. In addition to the aforementioned weaknesses, this solution is not economical and makes the problem highly intricate to solve. However, another solution that is more efficient and does not make the problem too large is discretization of the elements locally. This means that the elements with over permissible errors are refined, but the elements with permissible errors remain unchanged. This method is known as Adaptive Refinement. However, this method requires a parameter by which the local error of all elements should be computed. This parameter is known as $\boldsymbol{\xi}_i$.

Although the relative percentage error written by Eqs. (50) and (53) are defined on the whole domain, it is noteworthy that the square of each can be obtained by summing element contributions. Thus:

$$\left\|\boldsymbol{e}^*\right\|^2 = \sum_{i=1}^{m} \left\|\boldsymbol{e}_i^*\right\|^2, \tag{55}$$

where i represents an element contribution, and m is designated the total element number. In fact, for an 'optimal' mesh, we generally try to equate the contributions to this square of the norm for all elements [4–12]. Thus, in the $\boldsymbol{J}$ norm, the following equations can be written:

$$\left\|\boldsymbol{e}^*\right\|^2 = m \cdot \left\|\boldsymbol{e}_i^*\right\|^2, \tag{56}$$

$$\eta = \left[\frac{m \cdot \left\|\boldsymbol{e}_i^*\right\|^2}{\|\boldsymbol{J}^*\|^2 + \|\boldsymbol{e}^*\|^2}\right]^{1/2} \times 100\%, \tag{57}$$

$$\eta = \bar{\eta} \Rightarrow \left\|\boldsymbol{e}_i^*\right\| = \left\|\boldsymbol{e}_{\text{per}}^*\right\|, \tag{58}$$

where $\left\|\boldsymbol{e}_{\text{per}}^*\right\|$ denotes the permissible error norm for each element. If Eqs. (57) and (58) are combined, then the following equations are obtained:

$$(\bar{\eta})^2 = \frac{m \cdot \left\|\boldsymbol{e}_{\text{per}}^*\right\|^2}{\|\boldsymbol{J}^*\|^2 + \|\boldsymbol{e}^*\|^2}, \tag{59}$$

$$\left\|\boldsymbol{e}_{\text{per}}^*\right\| = \frac{\bar{\eta}}{\sqrt{m}}\left[\left\|\boldsymbol{J}^*\right\|^2 + \left\|\boldsymbol{e}^*\right\|^2\right]^{1/2}. \tag{60}$$

According to the definition, ratio $\boldsymbol{\xi}_i$ is as follows:

$$\boldsymbol{\xi}_i = \frac{\left\|\boldsymbol{e}_i^*\right\|}{\left\|\boldsymbol{e}_{\text{per}}^*\right\|}. \tag{61}$$

Therefore, as a criterion, if $\boldsymbol{\xi}_i < 1$, the error of the i th element is acceptable, but if $\boldsymbol{\xi}_i > 1$, the error of the i th element is over permissible.

In general, local refinement operations of mesh generation are carried out based on one of the following methods:

1. h-refinement (which achieves accuracy by refining the mesh using a given type of finite element); the first of these methods is element subdivision (enrichment);
2. p-refinement (which increases the order of polynomial trial function approximation in a pre-defined element subdivision);
3. h–p-refinement (which is the proper combination of h-and p-refinements);

The 2nd and 3rd aforementioned procedures have particular advantages in many (elliptic) situations when combined with a *hierarchic formulation*. The efficiency of these procedures involves, generally, abandoning a standard finite element structure. Consequently, in the present study, h-refinement and enrichment mesh generation is used such that the mesh generation structure is maintained during the refinement process and refinement operations are carried out merely over the elements with higher errors.

Mesh generation includes two interrelated generation tasks of well-placed nodes on the boundary and in the interior of the domain, and the triangulation of these nodes. As the distribution of the nodes clearly influences the nature of the mesh obtained, the placement of these nodes is a significant step in this algorithm.

The problem of placing nodes in a domain to obtain a satisfactory triangular mesh can be approached in a number of ways. In this study, the nodes are conveniently divided into two disjoint sets, namely, boundary nodes and interior nodes. The boundary nodes are those which lie on the outside boundary of the object domain and on the boundaries of any interior holes. The interior nodes are those lying inside the domain.

In this research, the major steps involved in adaptive mesh generation are:

(a) At first, the problem is analyzed using the finite element method and by the three-node triangular element.

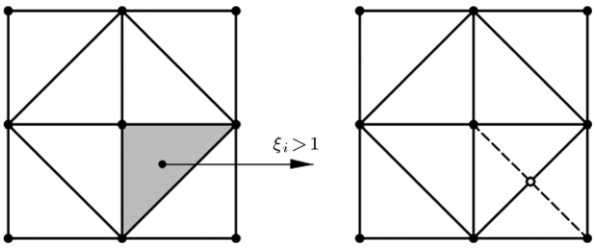

Figure 4: Placement of additional node for mesh refinement.

(b) Overall relative error (η) and local relative error ($\boldsymbol{\xi}_i$) are calculated based on equations introduced in the previous sections.
(c) The elements with $\boldsymbol{\xi}_i > 1$ are divided into two elements, creating an additional node in the middle of the longer side. In this step, due to the additional node in the middle of the longest side of the triangular element, the other triangular element connected to the longest side can compulsorily be divided into two elements (see Figure 4).
(d) The new refined mesh is analyzed again by the finite element method and step (b) is repeated. This process is continued until $\boldsymbol{\xi}_i < 1$ for all elements.
(e) When $\boldsymbol{\xi}_i < 1$ for all elements, the solution is stopped and all internal actions can be calculated by analyzing the last refined mesh generation.

By using enrichment mesh generation during the *h*-refinement process, the following points have been considered:

1. In parametric studies based on the step by step method (from step (a) to step (e)), it was observed that several elements have no suitable sizes due to their division into smaller ones. Therefore, a criterion was added to the criterion of division in step (c). According to this criterion, the elements, in which the ratio of the longest side to the height is larger than a constant number (for example 6), are also divided into two elements.
2. At the beginning of the solution in the *h*-refinement process, using enrichment mesh generation, if the sizes of the elements are not selected properly (which mostly occurs), $\boldsymbol{\xi}$ in some elements, can become much smaller than one. Moreover, in several others, it reaches near one and, in the rest, much larger than one (for example larger than 15). Hence, in the criterion of division, it was predicted that in the first analysis, $\boldsymbol{\xi}$ is compared with a larger number than one to distribute the elements uniformly and, as the number of analyses increases, $\boldsymbol{\xi}$ tends to reach one, such that $\boldsymbol{\xi}$ for all elements should be smaller than one in the last analysis. The above method is more efficient in parametric studies.
3. As it was noted in step (c), due to an extra node in the middle of the longest side of an element, several other elements can be compulsorily divided into two elements. In a particular situation, although an element does not need to be divided in itself, it can be divided into smaller elements because of its connected elements. For instance, in Figure 5, it is supposed that element two does not require to be divided, but elements one and three are required to be refined. In addition, it is supposed that the longest side of elements one and three is attached to the second element. Thus, based on step (c), although element two does not need to be divided, it should be divided into three elements, due to elements one and three, which are attached to it.

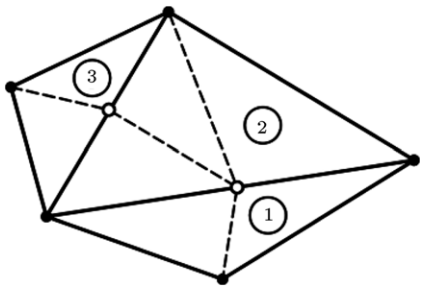

Figure 5: The compulsory division of the element number 2 into more than two elements in the mesh refinement process.

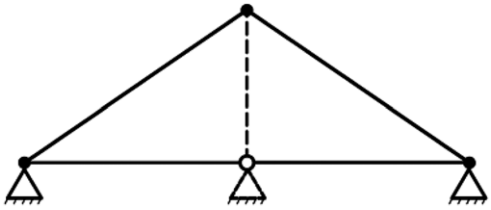

Figure 6: Restraining of the extra boundary node's freedom in the mesh refinement process.

4. If two out of three nodes of a three-node triangular element are restrained and its $\boldsymbol{\xi}$ is larger than one, it should be considered that if the extra node is in the middle of the side connected to restrained nodes, the degrees of freedom of the defined extra node should further be restrained (see Figure 6).

5. Determination of ultimate load and possible failure path using adaptive refinement process

In general, refinement methods for the non-linear solution of problems in continuous domains are created by joining the following packages of software:

1. Preparing non-linear analysis software.
2. Preparing a software to calculate overall relative error (η) and local relative error ($\boldsymbol{\xi}_i$).
3. Preparing software for the refinement of mesh generation based on the defined error norm.

In non-linear analysis, one may question the suitable timing for performing the refinement method. The following choices provide the answers to the question:

- Performing the refinement method at the end of each iteration analysis.
- Performing the refinement method at the end of each load step.

But, since at the end of each iteration analysis, the internal and external forces are not equilibrant, the refinement method is not performed at the end of each iteration analysis. Thus, the ending of each load step is the appropriate timing for performing the refinement method in non-linear analysis.

At the end of each load step, the refinement operation can be stopped, based on one of the following criteria:

1. The refinement operation is stopped after obtaining $\eta < \bar{\eta}$ at the end of each load step.
2. The operation is stopped after obtaining $\boldsymbol{\xi}_i \leq 1$ for all elements.

3. The operation is stopped after a certain number of adaptive refinement processes in each load step.

Selecting each of the above criteria causes an increase or decrease in the analysis timing, and further causes the probable failure path to become either thinner or thicker.

In the present research, the following step by step method is used to determine the ultimate load and the possible failure path:

1. At first, by using non-linear analysis software and the solution of the problem with fewer numbers of elements and an initial mesh, the ultimate load is approximately estimated by a trial and error method and the load coefficients and the required numbers of load steps are specified.
2. In each load step, the following steps are followed, respectively:
   2.1 At first, the problem undergoes a non-linear analysis for the specified load step.
   2.2 The (η) value for the entire domain and the ξ_i value for all elements are computed by the appropriate software and based on previously described methods.
   2.3 Based on ξ_i values, the existing mesh is refined by the appropriate software.
   2.4 The new refined mesh is again analyzed and returns to step 2.2. This process continues until one of the stop criteria is obtained (at the user's will). The results and the ultimate mesh are saved.
3. The refinement operation for all load steps is performed according to step 2.
4. The number of load steps, the load coefficient value in different load steps and the convergence of the solution, in particular in the final steps, are evaluated, and, if there is any problem with the convergence, the number of load steps and the load coefficient value in different load steps are refined and the problem is analyzed again from step 1.
5. The load–displacement curve is drawn to control the number of load steps and the load coefficient value in different load steps, and if the ratio of displacement in the last load step to elastic displacement is sufficiently large, the operation will be stopped.

6. Numerical examples

Example 1 (*A Rigid and Rough Strip Surface Footing*)**.** This example, as seen in Figure 7, has been chosen to demonstrate the combination of adaptive refinement and mesh smoothing using a "remesh and reanalyze" adaptive process. In this example, by using the energy norm, ultimate load and the possible failure path for a rigid and rough strip surface footing are determined. The ultimate load value is obtained by the adaptive finite element method, with values obtained from different theories that have also been compared.

In this example, the plane strain conditions are assumed with the following information:

$E = 21$ MPa (Yong's modulus)
$\nu = 0.30$ (Poisson's ratio)
$H' = 0$ (Plastic hardening modulus)
C= 24 kPa (Cohesion)
$\varnothing = 0$ (Angle of internal friction)
$B = 8$ m (Width of footing)
Yield criteria = Mohr–Coulomb criterion.

For surface footing, as shown in Figure 7, the adaptive refined mesh and contours of the distribution of the energy norm error estimator at the end of different load steps have been illustrated in Figure 8. The color scheme used in the adaptive refined meshes (Figure 8 and other similar figures) represents

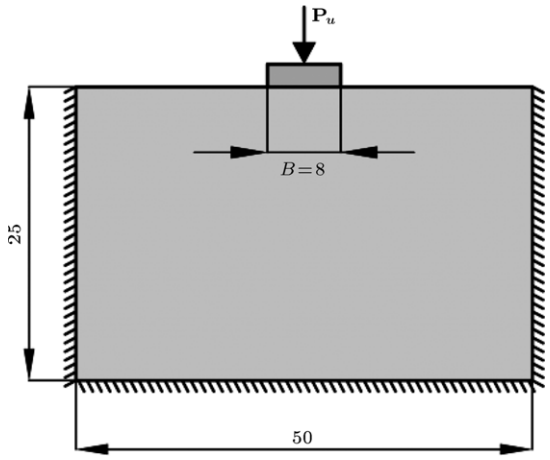

Figure 7: Physical model of a rigid and rough strip surface footing.

the relative percentage error in each element, and has been adjusted as follows:

ξ_i<0.9	ξ_i<1.0	ξ_i<1.1	ξ_i<1.3	ξ_i<1.5	ξ_i<1.8	ξ_i<2.5	ξ_i<5.0	ξ_i<10	ξ_i>10

Figure 9 shows variations of ultimate load and vertical displacement in the center of the strip footing, and comparison of ultimate load with values obtained from different theories

- Bell's theory: $P_u = 4 \times B \times C$
- Hansen's theory: $P_u = 5.14 \times B \times C$
- Terzaghi's theory: $P_u = 5.7 \times B \times C$
- Adaptive F.E.M.: $P_u = 5.82 \times B \times C$

where:

C = Cohesion
B = Width of footing.

Example 2 (*A Deep Cantilever Beam with a Rigidly Fixed Side*)**.** This example, as seen in Figure 10, has been chosen to demonstrate a combination of adaptive refinement and mesh smoothing using a "remesh and reanalyze" adaptive process. In this example, by using the ***J*** norm, the increased coefficient of the material weight and possible failure path for a deep cantilever beam is determined. In this example, the plane stress conditions are assumed, with the following information:

$E = 2 \times 10^5$ MPa (Yong's modulus)
$\nu = 0.30$ (Poisson's ratio)
$H' = 0$ (Plastic hardening modulus)
$\sigma_y = 240$ MPa (Yield stress)
$\gamma = 0.1$ (Unit weight material)
Yield criteria = Von Mises criterion.

For the above numerical example, the adaptive refined mesh and contours of the distribution of the ***J*** norm error estimator at the end of different load steps have been presented in Figure 11. The direction of minimum principle stresses at the center of elements in the last load step, and variations of the increased coefficient of material weight and vertical displacement at point A, have been presented in Figures 12 and 13, respectively.

Example 3 (*Adaptively Refined Final Mesh Results Obtained Through* ***J*** *and Energy Norms*)**.** For the illustrated problem in Example 2, Figure 14(a) and (b) show the comparison of adaptively refined final mesh results obtained through ***J*** and energy norms, respectively. These figures are related to the adaptively refined mesh in the latest load step.

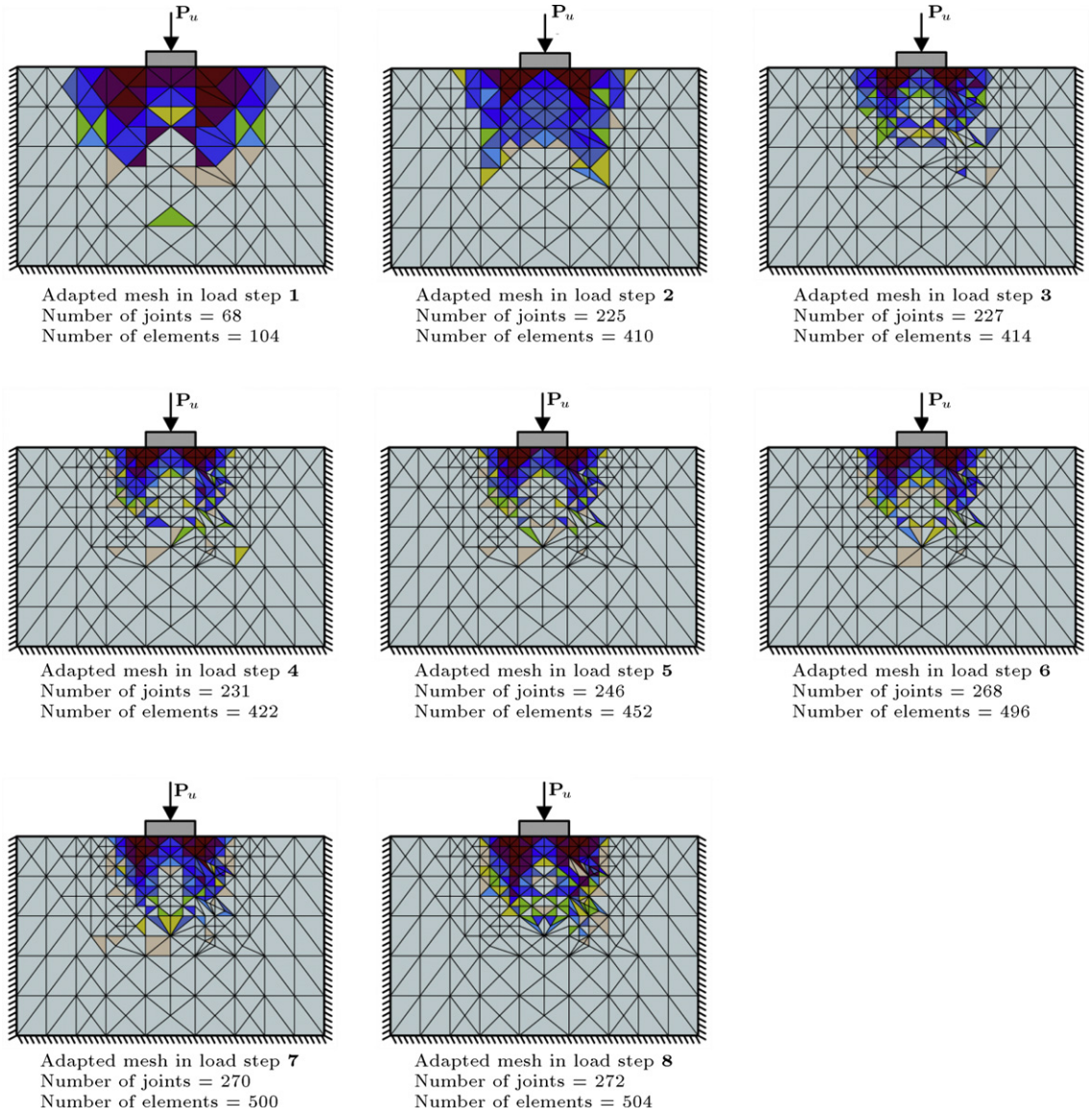

Figure 8: Adaptive refined mesh and contour of the distribution of the energy norm error estimator at the end of different load steps.

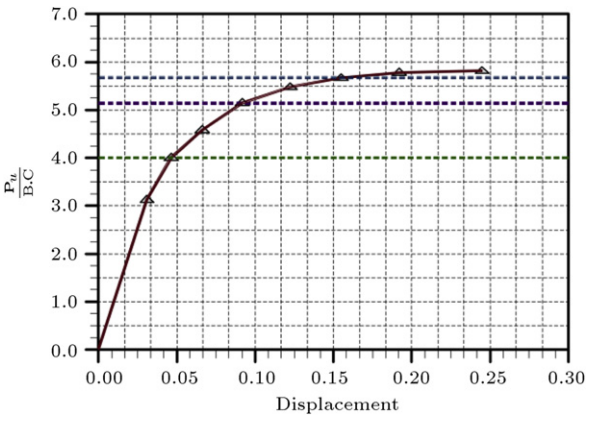

Figure 9: Variations of ultimate load and vertical displacement at the center of strip footing and comparison of the ultimate load with values obtained from different theories.

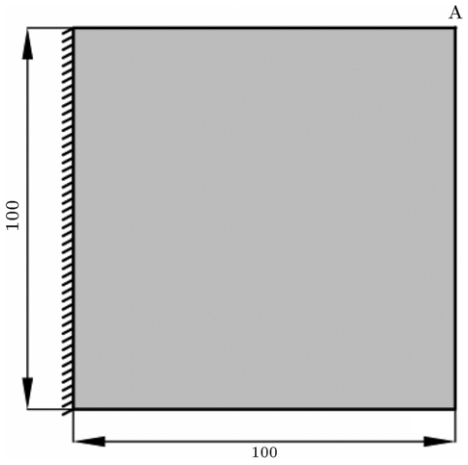

Figure 10: Physical model of a deep cantilever beam with a rigidly fixed side.

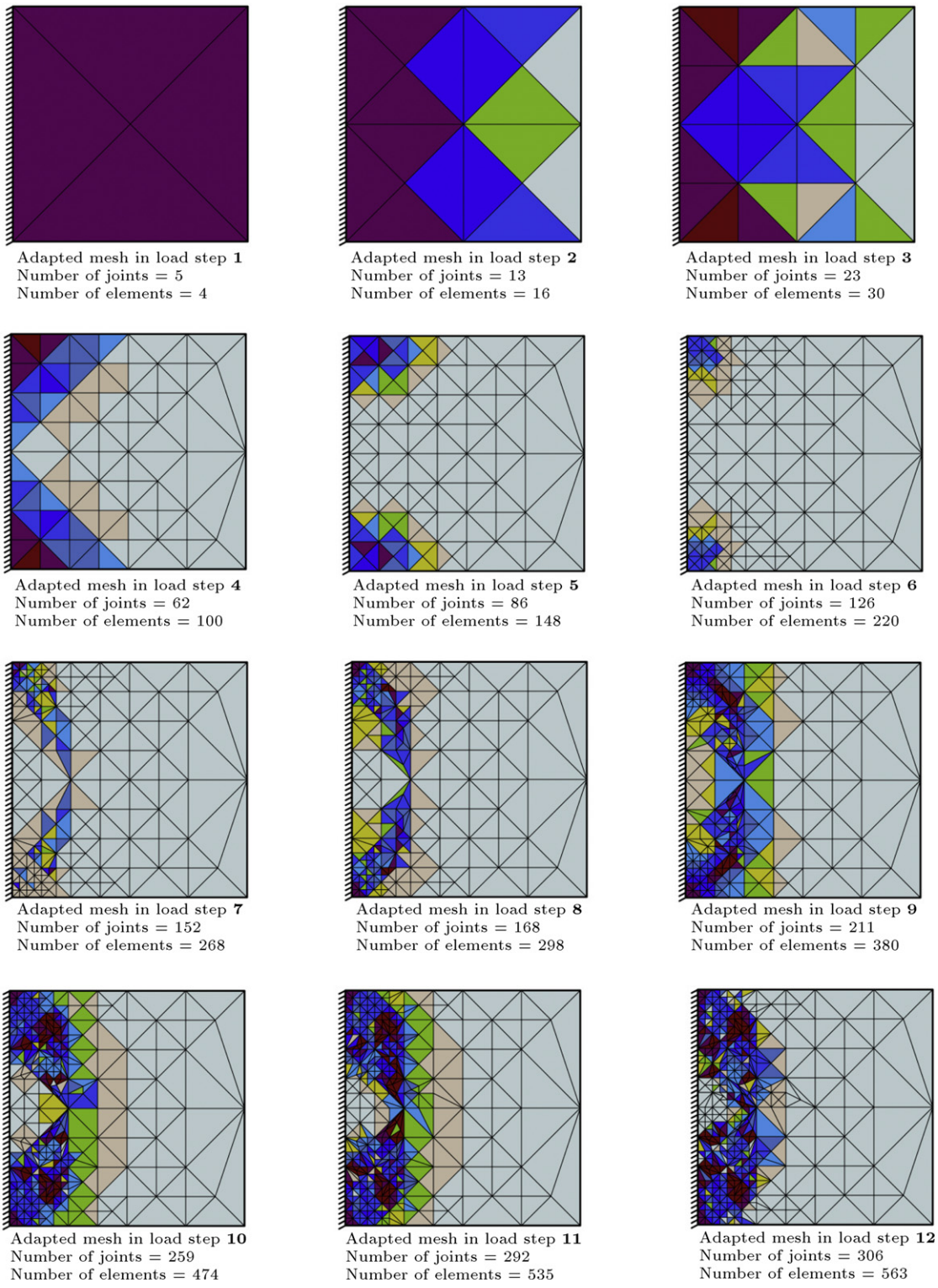

Figure 11: Adaptive refined mesh and contour of the distribution of the $\boldsymbol{J}$ norm error estimator at the end of different load steps for the deep cantilever beam as illustrated in Figure 10.

7. Conclusion

In the present research, the finite element method was primarily presented as a general technique for the numerical solution of a variety of problems encountered in engineering. However, this method has several limitations, such as being unaware of the suitability of element sizes, being unaware of the error value in the process of discretization, having no precise information about the propagation of the failure path and having costly access to the formation path of the

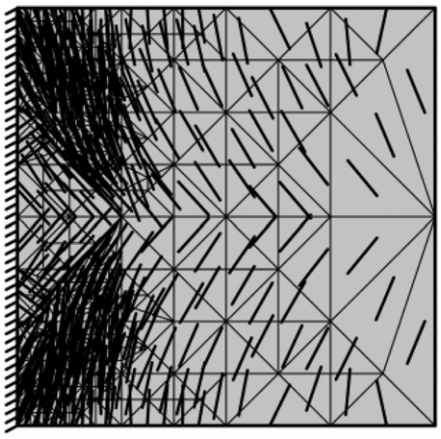

Figure 12: Direction of minimum principle stresses in the center of elements in the last load step for the deep cantilever beam as shown in Figure 10.

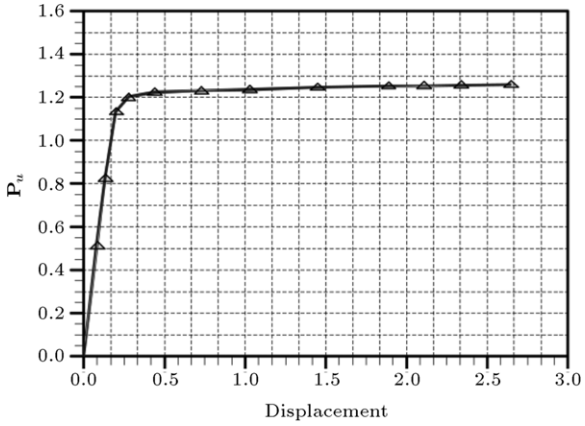

Figure 13: Variations of increased coefficient of material weight (α) and vertical displacement at point **A** for the deep cantilever beam as displayed in Figure 10.

failure mechanism. In order to overcome the aforementioned limitations, the adaptive finite element method was presented as an efficient method.

The advantages of the adaptive finite element method over the general finite element method are as follows:

1. The computation of overall relative error (η), based on the rule of gradient recovery, and its comparison with acceptable overall relative error ($\bar{\eta}$), to control the solution accuracy.
2. The computation of local relative error ($\boldsymbol{\xi}_i$) for all elements in order to obtain their proper sizes.
3. Possible adaptive refinement of mesh based on the local relative error ($\boldsymbol{\xi}_i$) is computed for all elements. In this stage, the local error estimate is used to steer the discretization process and the global error estimate is employed as a stopping criteria.
4. Accessing the failure mechanism with much fewer elements. Considering the adaptive finite element method, the refinement operations are only exerted in areas where the error rate is high. Thus, it is possible to obtain the ultimate load with much fewer elements.
5. Accessing the possible failure paths through adaptive refinement of the elements; given the fact that the relative local error rate in the failure propagation paths is high, the actual size of the elements in these areas will be smaller than those in other areas. Therefore, the element size distribution at each load step represents propagation of the failure path in the adaptive finite element analysis.

In previous studies, the estimation of the error rate in the non-linear solution of continuous domains problems with the adaptive finite element method was generally accomplished by the error computation of L_2 for stress, L_2 for strain, and energy norms. What makes this study distinct from previous similar ones is its simplicity and efficiency in the non-linear solution of problems (such as modeling a rigid connection in steel structures, in order to estimate the rotation of connection in leveling positions, and to define the plastic joint formation position) and, further, in involving yield criteria concepts, such as von Mises, Tresca, Mohr–Coulomb, and other yield criteria, to estimate error and adaptive refinement strategies in order to determine the ultimate load and the possible failure path in continuous domains problems.

Example 1 has been chosen in order to compare the results of this study with known theories. Since, in the finite element method, the obtained response is a level high, and considering that the difference between the response of the adaptive finite element method and that of existing theories is relatively lower, the obtained results can be considered acceptable due to the assumptions used in the finite element method, which

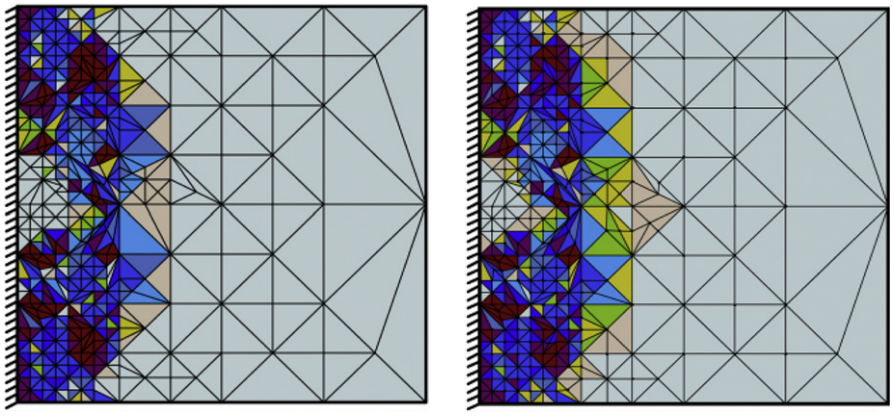

(a) $\boldsymbol{J}$ norm. Number of joints = 306. Number of elements = 563.

(b) Energy norm. Number of joints = 320. Number of elements = 591.

Figure 14: Comparison of adaptively refined final mesh results obtained via $\boldsymbol{J}$ and Energy norms for the deep cantilever beam as presented in Figure 10.

is considered to be acceptable. It should be noted that the aforementioned approximate theories provide users with no information about the propagation of the failure path. In other words, these theories do not show where the failure starts and in which sites the displacements are more than others. Based on the simple and effective method used in this study, in addition to accessing the ultimate load, it is possible to access the propagation path of the failure mechanism as well. The above information is highly useful to prevent failure.

The similarity of the results obtained in Example 2 in which the propagation of the failure path of a deep cantilever beam is shown, with the formation of the plastic flexural strength of a deep cantilever beam, represents one of the strengths of the adaptive refinement in the finite element method analysis. As displayed in Example 2, according to the method used in this study, the access to the ultimate load and failure path formation is possible with a highly simple, effective and inexpensive method.

Parametric studies in this research revealed that access to the ultimate load and the probable failure path is possible through any of L_2 for stress, L_2 for strain, energy, and $\boldsymbol{J}$ norms. However, as displayed in Example 3, selecting $\boldsymbol{J}$ norm primarily causes possible access to the failure mechanism with relatively fewer numbers of elements, and secondly, the $\boldsymbol{J}$ norm displays that the quality of the probable failure path is better than that of the energy norm. However, the quality and the reliability of the error estimator are obviously dependent on the accuracy of the recovered solutions, and, eventually, on the smoothing procedures.

One of the weaknesses observed in the examples analysis was inaccessibility to the thin and regular failure bond. At the first look, the reason seemed to depend on the type of norm selected. However, studies and investigations into different norms demonstrated that disregarding large deformations and large strains in non-linear analysis was the main reason for inaccessibility to the thin and regular failure bond. Hence, to obtain the thin and regular failure bond, it is necessary to consider large deformations and large strains in non-linear analysis.

Acknowledgments

The authors gratefully acknowledge the help and comments of AH Gandomi (The University of Akron).

References

[1] Babuska, I. and Rheinboldt, W.C. "Error estimates for adaptive finite element computations", *SIAM J. Numer. Anal.*, 15, pp. 736–754 (1978).
[2] Babuska, I. and Rheinboldt, W.C. "A posteriori error estimators for the finite element method", *Int. J. Numer. Methods Eng.*, 12, pp. 1597–1615 (1978).
[3] Bank, R.E. and Weiser, A. "Some a posteriori error estimators for elliptic partial differential equations", *Math. Comp.*, 44, pp. 283–301 (1985).
[4] Zienkiewicz, O.C. and Zhu, J.Z. "A simple error estimator and adaptive procedure for practical engineering analysis", *Int. J. Numer. Methods Eng.*, 24, pp. 337–357 (1987).
[5] Ainsworth, M., Zhu, J.Z., Craig, A.W. and Zienkiewicz, O.C. "Analysis of the Zienkiewicz–Zhu *a*-posteriori estimator in the finite element method", *Int. J. Numer. Methods Eng.*, 28, pp. 2161–2174 (1989).
[6] Zienkiewicz, O.C. and Zhu, J.Z. "Error estimates and adaptive refinement for plate bending problems", *Int. J. Numer. Methods Eng.*, 28, pp. 2839–2853 (1989).
[7] Zienkiewicz, O.C., Zhu, J.Z. and Gong, N.G. "Effective and practical *h–p* version adaptive analysis procedures for the finite element method", *Int. J. Numer. Methods Eng.*, 28, pp. 879–891 (1989).
[8] Zienkiewicz, O.C. and Huang, G.C. "A note on localization phenomena and adaptive finite element analysis in forming processes", *Commun. Appl. Numer. Methods*, 6, pp. 71–76 (1990).
[9] Zienkiewicz, O.C. and Zhu, J.Z. "Adaptive and mesh generation", *Int. J. Numer. Methods Eng.*, 32, pp. 783–810 (1991).
[10] Zienkiewicz, O.C. and Zhu, J.Z. "The superconvergent patch recovery and *a*-posteriori error estimates, part 1: the recovery technique", *Int. J. Numer. Methods Eng.*, 33, pp. 1331–1364 (1992).
[11] Zienkiewicz, O.C. and Zhu, J.Z. "The superconvergent patch recovery and *a*-posteriori error estimates, part 2: error estimates and adaptivity", *Int. J. Numer. Methods Eng.*, 33, pp. 1365–1382 (1992).
[12] Zienkiewicz, O.C. and Zhu, J.Z. "The superconvergent patch recovery (SPR) and adaptive finite element refinement", *Comput. Methods Appl. Mech. Engrg.*, 110, pp. 207–224 (1992).
[13] Boroomand, B. and Zienkiewicz, O.C. "Recovery by equilibrium in patches (REP)", *Int. J. Numer. Methods Eng.*, 40, pp. 137–164 (1997).
[14] Boroomand, B. and Zienkiewicz, O.C. "An improved REP recovery and the effectivity robustness test", *Int. J. Numer. Methods Eng.*, 40, pp. 2347–3277 (1997).
[15] Diez, P., Rodenas, J.J. and Zienkiewicz, O.C. "Equilibrated patch recovery error estimates: simple and accurate upper bounds of the error", *Int. J. Numer. Methods Eng.*, 69(10), pp. 2075–2098 (2007).
[16] Asghari, A. "Determination of ultimate load and possible failure lines for continuous media using adaptive finite element method", *Ph.D. Thesis*, Tehran University, Tehran, Iran (2001).

Abazar Asghari received his B.S. degree in Civil Engineering from Isfahan University of Technology, Isfahan, Iran, and his M.S. and Ph.D. degrees in Structural Engineering from the School of Civil Engineering, College of Engineering, at Tehran University, Iran. Dr Asghari is a faculty member of the Department of Civil Engineering in Urmia University of Technology, Iran. His research interests include error measure and mesh refinement in the finite element analysis, seismic resistance design of buildings and dynamic of structures.

Rasoul Mirghaderi is a faculty member of the School of Civil Engineering, College of Engineering, at Tehran University, Iran. He received his Ph.D. degree from Purdue University. He served as Supervisor and Representative of the Applied Research Department of the University of Tehran in this research. He is also a permanent member of the committee for revising the national code of practice for the seismic resistance design of buildings.